Journal of Materials Chemistry C

Accepted Manuscript

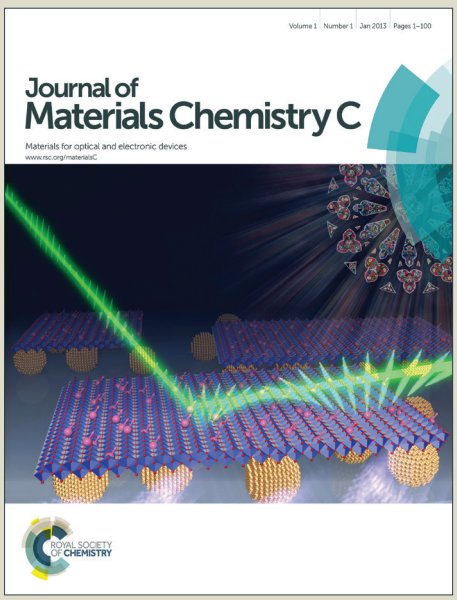

ROYAL SOCIETY OF CHEMISTRY

www.rsc.org/materialsC

Journal of Materials Chemistry C

RSCPublishing

ARTICLE

Reduced efficiency roll-off in all phosphorescent white organic light-emitting diodes with an external quantum efficiency of over 20%

Cite this: DOI: 10.1039/x0xx00000x

Liping Zhu, Zhongbin Wu, Jiangshan Chen and Dongge Ma*

Received 00th January 2012,
Accepted 00th January 2012

DOI: 10.1039/x0xx00000x

www.rsc.org/

Although previously reported all phosphorescent white organic light-emitting diodes (WOLEDs) exhibit impressive electroluminescence efficiency, problems remain in terms of the severe efficiency roll-off at high brightness. Here, a smart design in emissive zone structure is presented to make full use of generated excitons to realize high efficiency all phosphorescent WOLEDs with reduced efficiency roll-off. The fabricated WOLEDs show a maximum power efficiency (PE) of 46.6 lm/W, a current efficiency (CE) of 46.4 cd/A and an external quantum efficiency (EQE) of 22.4%, and yet remain as high as 41.3 lm/W, 46.2 cd/A and 22.0%, respectively, at the brightness of 1000 cd/m^2, exhibiting less pronounced efficiency roll-off. The critical current density, where EQE declines by half from its peak, reaches 220 mA/cm^2, which should be a higher value for all phosphorescent WOLEDs with an external quantum efficiency of over 20%.

1. Introduction

White organic light-emitting diodes (WOLEDs) are of great advantages for their potential applications in next generation full-color flat-panel displays and solid-state lighting sources for their merits of flexibility, large area, tunable color, etc.[1, 2, 3] The use of phosphors has become indispensable to realize high efficiency WOLEDs owning to their ability to achieve nearly 100% internal quantum efficiencies by harvesting both singlet and triplet excitons.[4, 5] Usually, all phosphorescent WOLEDs with high color rendering index (CRI) can be realized by constructing two architectures, including a single-emissive-layer (single-EML)[6] or multi-emissive-layer (multi-EML)[2, 7-10] with complementary of three primary color emitting dopants. The balanced white light emission can be well achieved by careful adjustment in the doping concentration or the thickness of EML. In the single-EML structures, the phosphors with longer wavelength (i.e. orange or red phosphors) are usually doped in a very low concentration, which increases the difficulty to control the doping ratio and the white emission spectra. Comparatively, the multi-EML structures are relatively easier to control the doping concentration and the exciton recombination zone, thus realizing high efficiency and high CRI while keeping the stable white emission. However, the efficiency roll-off at high brightness in all phosphorescent WOLEDs based multi-EML structures still exists, which is especially important for the application of WOLEDs in lighting. Therefore, it is urgently expected to find smart methods to resolve this problem.

The efficiency roll-off in OLEDs is mainly due to the exciton losses to become more and more serious at high brightness. Generally, a concept of critical current density J_0, defined as the point where the quantum efficiency is reduced to half of its maximum value, is used to express the degree of efficiency roll-off.[11] The mechanisms responsible for the roll-off are mainly separated into two general categories: a reduction in confinement of carriers in the EML and exciton quenching. The confinement of holes and electrons in EML will reduce at high driving current densities, resulting in a reduced fraction of carrier recombination in the EML, which will be an obstacle for high efficiency operation.[12] But such losses can often be eased

through the utilization of effective charge carrier blocking layers that confine the injected electrons and holes in the EML.[8, 13] As for the exciton quenching mechanism, the employment of long lifetime phosphorescent emitters will easily cause triplet-triplet annihilation (TTA) and triplet-polaron quenching (TPQ), both of which are strongly dependent on the local density of excitons.[12, 14] The efficiency roll-off in monochrome OLEDs has been greatly alleviated by using the exciton and carrier confinement structures, extending the width of exciton recombination zone,[15, 16] and reducing the lifetime of the iridium emitter.[4] However, the complicated device structures of WOLEDs greatly increase the difficult degree to reduce the efficiency roll-off.[3, 17] At present, the best J_0 of 174 mA/cm^2 was achieved in a high efficiengy hybrid WOLED.[18] For high efficiency all phosphorescent WOLEDs, this value is as low as 59.3 mA/cm,[17] which is indeed expected to be further improved. In this paper, we present a highly smart design in device structure to greatly reduce the efficiency roll-off in all phosphorescent WOLEDs. We fabricated red, green and blue three EMLs in sequence to effectively control the exciton recombination zone by strategically selecting the hosts in EMLs. In our devices, a hole-type host is used in red and green emission region and a bipolar-type host is used in blue emission region. The fabricated WOLEDs exhibits the maximum power efficiency (PE), current efficiency (CE) and external quantum efficiency (EQE) of 46.6 lm/W, 46.4 cd/A and 22.4%, respectively, and yet remain them as high as 41.3 lm/W, 46.2 cd/A and 22.0% at the brightness of 1000 cd/m^2. The devices also show high CRI of 83. The J_0 is calculated to be as high as 220 mA/cm^2, which should be the best result in high efficiency all phosphorescent WOLEDs.[17-19]

2. Experimental Section

2.1 Device fabrication

All the devices were grown on glass substrates pre-coated with a 180 nm thick indium tin oxide (ITO) that has a sheet resistance of 10 Ω per square. The ITO substrates were degreased in ultrasonic solvent bath and then dried at 120℃ for 30 minutes. Before loaded into the deposition chamber, the ITO surface was treated with UV-ozone for 15 minutes. All layers were grown in succession by thermal evaporation without breaking vacuum (5×10^{-4} Pa). The organics and metal oxide were evaporated at the rate in a range of 1-2 Å/s except that the evaporation rate of the sensing layer is 0.02 Å/s, and the metals were evaporated at the rate of 8-10 Å/s. The overlap between ITO and Al electrodes was 4 mm×4 mm, which is the active emissive area of the devices.

2.2 Characteristics

The current–brightness–voltage characteristics were measured by using a Keithley source measurement unit (Keithley 2400 and Keithley 2000) with a calibrated silicon photodiode. The EL spectra were measured using a spectrascan PR650 spectro-photometer. All the measurements were carried out in ambient atmosphere.

3. Results and Discussion

3.1 Selection of materials and design of device structure

To fully utilize all excitons to realize 100% internal quantum efficiency (IQE) for light emission and effectively reduce efficiency roll-off at high brightness, it is very important to smartly design device structure, and therefore select proper materials to match it. Obviously, the highly effective injection and transport of charge carriers and the efficient confinement of formed excitons at a wide recombination region in the EML must be considered when designing device structure and selecting relative materials. In our all phosphorescent WOLEDs, we used molybdenum oxide (MoO_3)/ MoO_3 doped 4,4',4''-tri(N-carbazolyl)triphenylamine (TCTA) as the hole-injection and transport layer and lithium carbonate (Li_2CO_3) doped 1,3-bis(3,5-dipyrid-3-yl-phenyl)benzene (BmPyPB)/ Li_2CO_3 as the electron-transport and injection layer to realize the highly effective injection and transport of holes and electrons in EML,[20] and employed the intrinsic TCTA and BmPyPB layers near EML as the blocking layers to effectively confine the excitons in the EML due to their high triplet energy level (Table 1)[20]. For the design of EML, three-separated EMLs were anranged in the sequence of red, green and blue sequence from anode to cathode. The highly-efficienct phosphorescent emitters, iridium(III)bis(2-methyldibenzo-[f,h] quinoxaline)(acetylacetonate) (Ir(MDQ)$_2$(acac)), bis(2-phenylpyridine)iridium(III) (Ir(ppy)$_2$(acac)) and iridium(III)bis(4,6-(difluorophenyl)pyridinato- N, C$^{2'}$)picolinate (FIrpic) were used to emit the corresponding light of red, green and blue, which have been proven to achieve almost unity IQE in monochrome devices.[8, 13, 21] TCTA was used as the host for both red and green dopant, while a bipolar material, 26DCzPPy (2,6-bis(3-(carbazol-9-yl)phenyl)pyridine) was used as blue host. As shown, both of the used hosts show higher triplet level than the dopant (see Table 1), thus effectively avoiding the triplet exciton quenching from dopant to host. Using TCTA as both the hole transport layer (HTL) and host for the phosphorescent dopant eliminates the potential barrier at the HTL/EML interface completely.[22] And the almost aligned lowest unoccupied molecular orbital (LUMO) energy levels of 26DCzPPy (2.56 eV) and BmPyPB (2.62 eV) can ensure a barrier free electron injection. The bipolar host 26DCzPPy can help expanding exciton distribution, which will reduce the exciton collision in working device. Moreover, the structure of red, green and blue sequence EMLs is also favor in the formation of cascade energy transfer path, fully utilizing the formed excitons for light emission and color adjustment.

Evidently, the smart design in EML and device structure in our studies guarantees the realization of high efficiency all phosphorescent WOLEDs with reduced efficiency roll-off. The detailed device structure is depicted in Figure 1.

Table 1 Summary of the triplet level of the involved materials.

Materials	T_1 (eV)	Ref.
TCTA	2.83	8
26DCzPPy	2.71	8
BmPyPB	2.69	8
FIrpic	2.62	8
$Ir(ppy)_2(acac)$	2.4	18
$Ir(MDQ)_2(acac)$	2.0	3

3.2. Device performance

Through careful adjustment of the three emission layers and the adjacent functional layers, the optimized device with structure of ITO/MoO_3 (8 nm)/TCTA : MoO_3 (50%, 50 nm)/TCTA (25 nm)/TCTA:$Ir(MDQ)_2(acac)$(8%, 5 nm)/TCTA:$Ir(ppy)_2(acac)$ (6%, 2 nm)/26DCzPPy:FIrpic(20%, 5 nm)/BmPyPB (10 nm)/BmPyPB:Li_2CO_3 (3% , 30 nm)/Li_2CO_3 (1 nm)/Al was finished. As can be seen in Figure 2(a), the optimized device shows a turn-on voltage as low as 2.7 V , which is almost equivalent with the triplet energy level of the blue dopant (FIrpic, 2.62 eV), suggesting the effective injection of both holes and electrons from the electrodes into the EML.[23] The device exhibits a low operating voltage of 3.5 V and 4.1 V at 1,000 cd/m^2 and 5,000 cd/m^2, respectively. Figure 2(b) shows the maximum forward viewing PE, CE and EQE of 46.6 lm/W and 46.4 cd/A, 22.4%, which remain as high as 41.3 lm/W, 46.2 cd/A and 22.0% at a practical luminance of 1,000 cd/m^2, respectively, exhibiting less pronounced efficiency roll-off. Supposing the optical out-coupling efficiency is 20-30%,[24] the resulted EQE is corresponding to an internal EL quantum efficiency of almost 100%. This EL performance should be among the best results in the state-of-the-art all phosphorescent WOLEDs.[2, 7, 17] Table 2 summarizes the device performance in detail. Except such high EL efficiency, the resulting WOLEDs also show impressive reduced efficiency roll-off. As obtained, the J_0 reaches about 220 mA/cm^2, which is the highest value as compared to other phosphorescent WOLEDs containing Ir-based phosphors[17, 18, 25] while maintain such high efficiency as far as we know.

The normalized spectra at different luminance are showed in Figure 2(c), in which a good white emission with a CRI of 83 at 1,000 cd/m^2 is achieved. As the luminance increases, the relative intensity of blue emission increases and the red ratio decreases, the reason of the spectra variation will be discussed below. The Commission Internationale de L'Eclairage (CIE) coordinates at 1000 cd/m^2 is (0.45,0.44) with a corresponding correlated color temperature (CCT) about 2938 K, which is a desirable warm white illumination for lighting.

3.3. Location of recombination zone and emission mechanism

To realize the design concept of our WOLEDs, the control of the recombination zone location is of great importance which allows for the combination transporting properties of the hosts and dopants in EML. As described before, we used the red, green, blue sequence EML structure of TCTA:$Ir(MDQ)_2(acac)$(8%, 5 nm)/TCTA:$Ir(ppy)_2(acac)$ (6%, 2 nm)/26DCzPPy:FIrpic(20%, 5 nm). It is well-known that TCTA is a hole-dominated material with a hole mobility of 3×10^{-4} $cm^2V^{-1}s^{-1}$, which is much higher than its electron mobility of $< 10^{-8}$ $cm^2V^{-1}s^{-1}$.[26] Whereas 26DCzPPy is a bipolar material with approximately equivalent hole and electron mobility of 2×10^{-5} $cm^2V^{-1}s^{-1}$.[27] This means that the recombination zone should be mainly localized at the interface of TCTC:$Ir(ppy)_2(acac)$/26DCzPPy:FIrpic or in the blue EML. To determine the position of recombination zone in our WOLEDs, here we first constructed device 1 with the structure of ITO/MoO_3 (8 nm)/TCTA : MoO_3 (50%, 50 nm)/TCTA (27 nm) /TCTA (5 nm)/26DCzPPy:FIrpic(20%, 5 nm)/BmPyPB (10 nm)/BmPyPB:Li_2CO_3 (3%, 30 nm)/Li_2CO_3 (1 nm)/Al, and a 0.06 nm orange sensing layer of bis(2-phenylbenzothiozolato-N,$C^{2'}$) iridium(acetylacetonate) ($Ir(bt)_2(acac)$) was inserted into different positions of the 5 nm TCTA layer and the 26DCzPPy:FIrpic layer.[10] As demonstrated later, the red dopant $Ir(MDQ)_2(acac)$ in TCTA will not affect the hole transport properties, and the green dopant $Ir(ppy)_2(acac)$ will only slightly increase the hole transport, as reflected in the hole only devices (Figure 4(a) and (c)), indicating a very small impact on

Table 2. Comparison summary of WOLEDs with CRI above 80 and EQE over 20 %.

Ref.	V_{on} (V)	PE[a,b] (lm/W)	CE[a,b] (cd/A)	EQE[a,b] (%)	CIE[b]	CRI[b]	CCT[b]	J_0 (mA/cm^2)
2	2.8	59.9, 43.3	53.7, 49.6	23.3, 21.5	(0.43,0.43)	80.2	--	59.3
22	3.3	40.7, 37.1	49.6, 49.5	21.1, 20.0	(0.42,0.44)	85	3544	174
This work	2.7	46.6, 41.3	46.4, 46.2	22.4, 22.0	(0.45,0.44)	83	2938	220

[a]The maximum power efficiency (PE), current efficiency (CE), and external quantum efficiency (EQE)
[b]PE, CE, EQE, Commission Internationale de L'Eclairage coordinates (CIE), color rendering index (CRI) and correlated color temperature (CCT) at the luminance of 1000 cd/m^2

hole transporting after the emitter doping. The blue emitter is doped because the large doping concentration as high as 20% will change the transport property. The total thickness of the devices with $Ir(bt)_2(acac)$ thin layer is kept the same as that of the WOLEDs to maintain the same optical and electrical properties.[28] Figure 3(a) shows the normalized intensity of orange to blue emission in the devices with $Ir(bt)_2(acac)$ thin layer at the voltage from 3.5 V to 5.1 V. The interface of TCTA/26DCzPPy:FIrpic is set to be 0 nm. It can be seen that at the voltage range of 3.5-4.3 V, the maximum intensity of orange emission appears at TCTA/26DCzPPy:FIrpic interface, and sharply decreases in the TCTA layer to about 2 nm and gradually reduces in the 26DCzPPy:FIrpic layer up to about 5 nm, clearly showing the position and width of the exciton recombination zone in device 1. When the voltage further increases, the peak intensity of orange emission is deviated from the interface into the 26DCzPPy:FIrpic layer, indicating the slightly shifting of recombination zone into the blue EML zone with voltage. Clearly, in the case of device 1, the main exciton recombination zone is basically localized in the blue layer near to the TCTA/26DCzPPy:FIrpic interface.

However, as can be seen later, the green dopant $Ir(ppy)_2(acac)$ in TCTA will greatly enhance the electron transport current, thus affects the position of exciton recombination zone (Figure 4(d)). Therefore, we further fabricated the device 2 of ITO/MoO_3 (8 nm)/TCTA : MoO_3 (50%, 50 nm)/TCTA (27 nm)/TCTA:$Ir(ppy)_2(acac)$ (6%, 5 nm)/26DCzPPy:FIrpic(20%, 5 nm)/BmPyPB (10 nm)/BmPyPB:Li_2CO_3 (3%, 30 nm)/Li_2CO_3 (1 nm)/Al, which is more approximate to the WOLEDs in emission zone structure. The position of 0.06 nm $Ir(bt)_2(acac)$ sensing layer is yet changed as the previous device 1. Figure 3(b) depicts the normalized intensity of orange emission to both blue and green emission in device 2 at different voltages. It is clearly seen that an approximately symmetric intensity distribution with a peak at the position of 0 nm is obtained, and the relative orange intensity in the blue layer is reduced with respect to that in device 1, indicating the indispensible role of green dopant in TCTA in the redistribution of exciton density and the change of recombination zone. It is also concluded that the exciton recombination zone should be extended into the red emission layer in our WOLEDs considering the higher orange intensity in TCTA:$Ir(ppy)_2(acac)$ layer. (Figure 3(b) inset).

Regardless of whatever device architectures we design, the core to realize high efficiency WOLEDs is always involved by fine tuning of the charges and excitons that are associated with the physical processes within the devices, causing them to ultimately giving off efficient white light emission. So, it is pivotal to make a thorough inquiry of the emission mechanism in the WOLEDs we designed. Usually, in doped OLEDs, energy transfer and charge trapping are two main emission mechanisms. The dependence of current density-voltage (*J-V*) on guest concentration can be applied to distinguish the two emission mechanisms. For the charge trapping process, the dopant molecules may be considered as shallow trapping centers, which will trap the injected charge carriers and reduce the current density, resulting in a dependence of *J-V* characteristics on the doping concentration. For the energy transfer process, however, the *J-V* characteristics are not influenced by the variation of dopant concentration. To elucidate the electroluminescent processes of red, green and blue dopants in our WOLEDs, we investigated the current density-voltage characteristics of hole-only device ITO/MoO_3 (10 nm)/TCTA (40 nm)/Host or Host:dopant (x%, 40 nm)/TCTA (40 nm)/MoO_3 (10 nm)/Al (100 nm) and electron-only device ITO/Li_2CO_3 (1 nm)/BmPyPB (40 nm)/Host or Host:dopant (x%, 40 nm)/BmPyPB (40 nm) / Li_2CO_3 (1 nm)/Al (100 nm). For the case of $Ir(MDQ)_2(acac)$ and $Ir(ppy)_2(acac)$, the host is TCTA, whereas 26DCzPPy is used for the the host of FIrpic. Figure 4 shows their current density-voltage characteristics. It can be seen that the hole current unchanges and the electron current greatly decreases with the doping of $Ir(MDQ)_2(acac)$ in TCTA (Figure 4(a) and (b)). This means that $Ir(MDQ)_2(acac)$ possesses the role of very strong electron trapping, but not affects the hole transport in TCTA host. Differently, the doping of $Ir(ppy)_2(acac)$ in TCTA increases the electron and hole current simultaneously, and the increase in electron current is further obvious with respect to the hole current (Figure. 4(c) and (d)). This indicates that $Ir(ppy)_2(acac)$ doping in TCTA does not trap electrons or holes but helps the transport of both electrons and holes, which are very important for the profitable utilization of excitons and the effective suppression of TTA and TPQ in our WOLEDs. For the case of FIrpic doped 26DCzPPy-based device, the hole current increases while the electron current reduces after FIrpic doping (Figure 4(e) and (f)). This indicates that FIrpic doped in 26DCzPPy possesses the function of trapping electrons and transporting holes. On the basis of above transport processes, the emission mechanism of WOLEDs we fabricated can conclude well as follows. As described on the detailed emission processes of WOLEDs in Figure 1, the injected electrons from cathode and electron transporting layer will transport along the LUMO level of 26DCzPPy, the partial electrons will be trapped by FIrpic molecules and the others then transport into the green and red layers along the LUMO level of TCTA. As showed above, the green dopant accelerates the electron transport greatly in TCTA, and as the green EML is only 2 nm, the electrons can easily transport into the red emission layer. Due to the strong trapping effect of $Ir(MDQ)_2(acac)$, the electrons transported into the red layer will then be completely trapped by $Ir(MDQ)_2(acac)$ molecules. Since the doping in red, green and blue EMLs does not trap the holes, the injected holes from anode and hole-transporting layer then will easily transport along the highest occupied molecular orbital (HOMO) level of TCTA molecules in red and green EMLs, and into the blue EML due to the bipolar transport property of 26DCzPPy and the assistant of $Ir(ppy)_2(acac)$ in hole transport. Then the trapped electrons on FIrpic molecules will recombine with the transported holes, resulting in blue emission, whereas the trapped electrons on $Ir(MDQ)_2(acac)$ molecules recombine with the transported holes, finally leading to red emission. As for the thin green layer, although the partially transported electrons and holes on $Ir(ppy)_2(acac)$ molecules exist the possibility of direct

recombination to release green emission, it is believed that the energy transfer from blue layer should be main process for the green emission in our WOLEDs. The energy transfer from the green layer to the red layer is also quite efficient to contribute to the red emission.[2] Apparently, the thin green layer plays an important role in charge carrier transport and redistribution of excitons. Figure 5 gives the $Ir(ppy)_2(acac)$ concentration dependent spectra in our WOLEDs at 1000 cd/m^2. As is shown, the blue emission intensity decreases and the red emission increases as the doping concentration of $Ir(ppy)_2(acac)$ in TCTA increases, significantly changing the spectral properties of WOLEDs. This change demonstrates that there are more exciton energies to form in the red EML with the increase of $Ir(ppy)_2(acac)$ concentration, which is in accord with the increase of electrons transported into the red emission layer with $Ir(ppy)_2(acac)$ concentration, thus more exciton recombination in red EML.

3.4. Origin of low efficiency roll-off

The problem of efficiency roll-off at high luminance in phosphorescent OLEDs has been a bottleneck that is urgently needed to be settled.[15, 29] Supposing that the charge carrier and exciton confinement in our WOLEDs are effective considering the triplet exciton T_1 and energy levels of blocking layers, then the exciton quenching processes in emission layers will play a dominant role in the issue of efficiency roll-off, especially for the case of a large number of excitons accumulation in recombination zone. Usually, the excitons quench through two ways, i.e. TTA and TPQ, both of which are strongly dependent on the local exciton density. Luckily, the quenching processes are significantly suppressed in our WOLEDs by smartly designing in emission zone structure, as described above.

Besides the utilization of p-doped and n-doped transport layers, which will greatly enhance the charge carrier injection, the smart construction of reasonable emission zone is a key factor in enhancing the efficiency and reducing the efficiency roll-off in our WOLED. As we see in Figure 1, the same TCTA host is used in the red and green layers, which is also the same as the p-doped and hole-transporting layers, thus the holes injected from anode are very easy to transport into the red and green layers without any barrier, and finally transport easily into the blue emission layer due to the low interface barrier between TCTA and 26DCzPPy and the bipolar transport property of 26DCzPPy. Furthermore, the electrons injected from cathode are also very easy to transport into the blue EML due to the bipolar transport property of 26DCzPPy and the negligble barrier between 26DCzPPy and BmPyPB, and finally transport well into red emission layers by the significant assistant role of $Ir(ppy)_2(acac)$ molecules in accelerated the electron transport. And due to the strong electron trapping effect of $Ir(MDQ)_2(acac)$, the electron leakage from the red emission layer into the hole-transporting layer is also greatly suppressed, thus well confining the charge carriers within the whole EMLs. Additionally, the high T_1 levels of transporting layers and hosts also reduce the triplet exciton quenching and well confine the excitons in the EMLs. It can be seen that the designed emission zone structure well balances the charge carriers, effectively confines the excitons in wide recombination zone, greatly reduces the exciton accumulation and quenching, and well adjusts the non-uniformity of electric field contribution in emission layers. All these properties favor the enhancement of the efficiency and reduce of the roll-off.

It is found that the TTA model can well applied to fit our results, meaning that the efficiency roll-off at the high luminance in our WOLEDs is due to the TTA process. From another perspective, the inapplicable of TPQ model in the device suggest a well-balanced carrier injection and transportation, and the accumulated carriers in the EMLs are negligible, which is a further proof of the superiority in device design. For TTA model, the current density dependence of EQE can be expressed as:[10, 11]

$$\frac{\eta_{TT}}{\eta_0} = \frac{J_0}{4J}\left[\sqrt{1+8\frac{J}{J_0}}-1\right] \quad (1)$$

Where η_0 is the external quantum efficiency in the absence of triplet quenching, η_{TT} is in the presence of TTA, J_0 is the critical current density for TTA model. As shown in Figure 6, by fitting, we obtained the J_0 value as high as 220 mA/cm^2. This should be the highest value for the state-of-the-art all phosphorescent WOLEDs with an EQE of over 20%.[8, 17, 18]

4. Conclusion

In all, a high efficiency all phosphorescent WOLED was fabricated with three separated EML that shows excellent EL performance of maximum PE, CE and EQE of 46.6 lm/W, 46.4 cd/A and 22.4%, respectively, which slightly reduce to 41.3 lm/W, 46.2 cd/A and 22.0% at the luminance of 1000 cd/m^2. Such a high efficiency is attributed to the proper selection of materials and the smart design of the device structure to make full use of generated excitons. The recombination zone is well determined experimentally and spans the whole emission zone, which greatly reduces the exciton quenching. The emission mechanism of the fabricated WOLEDs is well explained by the detailed analysis in current-voltage characteristics of single carrier-only devices. It can be seen that the devices exhibit a higher external quantum efficiency of over 20% and the lower roll-off in efficiency with a J_0 value of 220 mA/cm^2, which should be the best result reported now in all phosphorescent WOLEDs with a CRI above 80. Our studies prove the possibility to further improve the efficiency roll-off at high luminance in all phosphorescent WOLEDs by carefully designing in device architecture to redistribute the charge carriers and excitons in recombination zone, thus greatly reducing the exciton quenching.

Acknowledgements

The authors gratefully acknowledge the National Natural Science Foundation of China (51333007, 91433201), Ministry of Science and Technology of China (973 program No. 2013CB834805), the Foundation of Jilin Research Council (2012ZDGG001, 20130206003GX), Chinese Academy of

Sciences (KGZD-EW-303-3), and CAS Instrument Project (YZ201103) for the support of this research.

Notes and references

Address: State Key Laboratory of Polymer Physics and Chemistry, Changchun Institute of Applied Chemistry, Chinese Academy of Sciences, Graduate University of the Chinese Academy of Sciences, Changchun 130022, People's Republic of China

1. S. Lee, H. Shin and J. J. Kim, *Adv. Mater.*, 2014, **26**, 5864-5868; Q. Wang and D. Ma, *Chem.Soc.Rev.*, 2010, **39**, 2387-2398.
2. Y.-L. Chang, Y. Song, Z. Wang, M. G. Helander, J. Qiu, L. Chai, Z. Liu, G. D. Scholes and Z. Lu, *Adv. Funct. Mater.*, 2013, **23**, 705-712.
3. G. Schwartz, S. Reineke, T. C. Rosenow, K. Walzer and K. Leo, *Adv. Funct. Mater.*, 2009, **19**, 1319-1333.
4. K. Udagawa, H. Sasabe, C. Cai and J. Kido, *Adv. Mater.*, 2014, **26**, 5062-5066.
5. C. Adachi, M. A. Baldo, M. E. Thompson and S. R. Forrest, *J. Appl. Phys.*, 2001, **90**, 5048-5051.
6. Q. Wang, J. Ding, D. Ma, Y. Cheng, L. Wang, X. Jing and F. Wang, *Adv. Funct. Mater.*, 2009, **19**, 84-95.
7. Q. Wang, J. Ding, D. Ma, Y. Cheng, L. Wang and F. Wang, *Adv. Mater.*, 2009, **21**, 2397-2401.
8. S. J. Su, E. Gonmori, H. Sasabe and J. Kido, *Adv. Mater.*, 2008, **20**, 4189-4194.
9. R. Wang, D. Liu, H. Ren, T. Zhang, H. Yin, G. Liu and J. Li, *Adv. Mater.*, 2011, **23**, 2823-2827.
10. L. Zhu, Y. Zhao, H. Zhang, J. Chen and D. Ma, *J. Appl. Phys.*, 2014, **115**, 244512.
11. M. A. Baldo, C. Adachi and S. R. Forrest, *Phys. Rev. B*, 2000, **62**, 10967-10977.
12. N. C. Giebink and S. R. Forrest, *Phys. Rev. B*, 2008, **77**, 235215.
13. D. Tanaka, H. Sasabe, Y.-J. Li, S.-J. Su, T. Takeda and J. Kido, *Jpn. J. Appl. Phys.*, 2007, **46**, L10-L12.
14. S. Reineke, K. Walzer and K. Leo, *Phys. Rev. B*, 2007, **75**, 125328; D. D. Song, S. L. Zhao, Y. C. Luo and H. Aziz, *Appl. Phys. Lett.*, 2010, **97**, 243304; W. Staroske, M. Pfeiffer, K. Leo and M. Hoffmann, *Phys. Rev. Lett.*, 2007, **98**, 197402.
15. N. C. Erickson and R. J. Holmes, *Adv. Funct. Mater.*, 2013, **23**, 5190-5198.
16. L. Deng, J. Li, G.-X. Wang and L.-Z. Wu, *J. Mater. Chem. C*, 2013, **1**, 8140; C.-H. Chen, L.-C. Hsu, P. Rajamalli, Y.-W. Chang, F.-I. Wu, C.-Y. Liao, M.-J. Chiu, P.-Y. Chou, M.-J. Huang, L.-K. Chu and C.-H. Cheng, *J. Mater. Chem. C*, 2014, **2**, 6183.
17. H. Sasabe, J.-i. Takamatsu, T. Motoyama, S. Watanabe, G. Wagenblast, N. Langer, O. Molt, E. Fuchs, C. Lennartz and J. Kido, *Adv. Mater.*, 2010, **22**, 5003-5007.
18. N. Sun, Q. Wang, Y. Zhao, D. Yang, F. Zhao, J. Chen and D. Ma, *J. Mater. Chem. C*, 2014, **2**, 7494-7504.
19. N. Sun, Q. Wang, Y. Zhao, Y. Chen, D. Yang, F. Zhao, J. Chen and D. Ma, *Adv. Mater.*, 2014, **26**, 1617-1621.
20. K. Walzer, B. Maennig, M. Pfeiffer and K. Leo, *Chem.Rev*, 2007, **107**, 1233-1271.
21. Y. L. Chang, Z. B. Wang, M. G. Helander, J. Qiu, D. P. Puzzo and Z. H. Lu, *Org. Electron.*, 2012, **13**, 925-931; C. W. Lee and J. Y. Lee, *Adv. Mater.*, 2013, **25**, 5450-5454.
22. Z. B. Wang, M. G. Helander, J. Qiu, D. P. Puzzo, M. T. Greiner, Z. W. Liu and Z. H. Lu, *Appl. Phys. Lett.*, 2011, **98**, 073310.
23. R. Meerheim, K. Walzer, G. He, M. Pfeiffer and K. Leo, *Proc. of SPIE*, 2006, **6192**, 61920P; H. Shin, S. Lee, K. H. Kim, C. K. Moon, S. J. Yoo, J. H. Lee and J. J. Kim, *Adv. Mater.*, 2014, **26**, 4730-4734; X. Zhou, M. Pfeiffer, J. S. Huang, J. Blochwitz-Nimoth, D. S. Qin, A. Werner, J. Drechsel, B. Maennig and K. Leo, *Appl. Phys. Lett.*, 2002, **81**, 922.
24. H. Uoyama, K. Goushi, K. Shizu, H. Nomura and C. Adachi, *Nature*, 2012, **492**, 234-238.
25. B. W. D'Andrade, R. J. Holmes and S. R. Forrest, *Adv. Mater.*, 2004, **16**, 624-628.
26. J.-W. Kang, S.-H. Lee, H.-D. Park, W.-I. Jeong, K.-M. Yoo, Y.-S. Park and J.-J. Kim, *Appl. Phys. Lett.*, 2007, **90**, 223508.
27. C. Cai, S.-J. Su, T. Chiba, H. Sasabe, Y.-J. Pu, K. Nakayama and J. Kido, *Org. Electron.*, 2011, **12**, 843-850.
28. J. Wünsche, S. Reineke, B. Lüssem and K. Leo, *Phys. Rev. B*, 2010, **81**, 245201.
29. D. Song, S. Zhao and H. Aziz, *Adv. Funct. Mater.*, 2011, **21**, 2311-2317; Q. Wang, I. W. H. Oswald, M. R. Perez, H. Jia, A. A. Shahub, Q. Qiao, B. E. Gnade and M. A. Omary, *Adv. Funct. Mater.*, 2014, **24**, 4746-4752; Q. Wang, I. W. Oswald, X. Yang, G. Zhou, H. Jia, Q. Qiao, Y. Chen, J. Hoshikawa-Halbert and B. E. Gnade, *Adv. Mater.*, 2014, **26**, 8107-8113; Q. Wang, I. W. H. Oswald, M. R. Perez, H. Jia, B. E. Gnade and M. A. Omary, *Adv. Funct. Mater.*, 2013, **23**, 5420-5428.

A rational design of the emission layers to achieve high efficiency WOLED with reduced roll-off.